Assessing and predicting the changes for inorganic mercury and methylmercury concentrations in surface waters of a tidal estuary (Adour Estuary, SW France)

Teodor Stoichev, Aubin Thibault de Chanvalon, Sandrine Veloso, Jonathan Deborde, Emmanuel Tessier, Laurent Lanceleur, David Amouroux

Marine Pollution Bulletin 186 (2023) 114400

Contents lists available at ScienceDirect

Marine Pollution Bulletin

journal homepage: www.elsevier.com/locate/marpolbul

Assessing and predicting the changes for inorganic mercury and methylmercury concentrations in surface waters of a tidal estuary (Adour Estuary, SW France)

Teodor Stoichev [a,*], Aubin Thibaut de Chanvalon [b], Sandrine Veloso [b], Jonathan Deborde [b,c], Emmanuel Tessier [b], Laurent Lanceleur [b], David Amouroux [b,*]

[a] Interdisciplinary Center of Marine and Environmental Research (CIIMAR/CIMAR), University of Porto, Terminal de Cruzeiros de Leixoes, Av. General Norton de Matos s/n, 4450-208 Matosinhos, Portugal

[b] Universite de Pau et des Pays de l'Adour, E2S UPPA, CNRS, IPREM, Institut des Sciences Analytiques et de Physico-chimie pour l'Environnement et les matériaux, Pau, France

[c] Ifremer, LITTORAL, Laboratoire Environnement Ressources des Pertuis Charentais, F-17390 La Tremblade, France

ARTICLE INFO

Keywords:
Effect separation
Contaminant transport
Pollution sources
Analysis of covariance
Mercury speciation
Water

ABSTRACT

Total and dissolved concentrations of inorganic mercury (IHg) and methylmercury (MeHg) in water (Adour Estuary) were determined during three sampling campaigns and related to biogeochemical variables (nutrients, organic matter). Factors (sampling time, sample type) were included in analysis of covariance with effect separation. The urban estuary suffered historically from anthropogenic sources, however, decreased emissions have reduced Hg concentrations. Total IHg (0.51–3.42 ng L^{-1}) and MeHg (25–81 pg L^{-1}) concentrations are additively described by suspended particulate matter and particulate organic carbon. Higher total concentrations, carried by organic-rich particles, were found near specific discharge points (0.79–8.02 ng L^{-1} and 34–235 pg L^{-1} for IHg and MeHg, respectively). The associated high dissolved MeHg concentrations could not be explained only by biogeochemical variables. Better efficiency of the models is found for total than for dissolved concentrations. Models should be checked with other contaminants or with estuaries, suffering from downstream contamination.

1. Introduction

The estuarine concentrations of mercury species have been studied more often in sediment and biological samples and less often in water, in spite of the importance of water compartment for the transport of contaminants (Navarro et al., 2012; Stoichev et al., 2018). The reasons are possibly related with difficulties in sample storage and analytical determinations of low levels of Hg species in water samples. The total concentrations of contaminants in estuarine waters depend on upstream river concentrations, lateral input and mixing between river and ocean water but also on in situ processes, such as sedimentation/resuspension phenomena. Total concentrations of Hg species are better predictor for their transport while dissolved concentrations, especially those of methylmercury, should represent more bioavailable forms. Riverine export is a very important source of both inorganic mercury (IHg) and methylmercury (MeHg) to coastal ocean, and, due to very high productivity, is able to affect MeHg concentrations in coastal species contributing to majority of human MeHg exposure (Liu et al., 2021). Furthermore, upon transition from rivers to coastal zone, sedimentation of fine and organic rich particles stimulates bacterial reduction of oceanic sulfate that may increase the net methylation of IHg (Azaroff et al., 2019; Stoichev et al., 2019). Mercury speciation studies in water from estuaries (Leermakers et al., 2001; Balcom et al., 2008; Wang et al., 2009; Bratkič et al., 2013; Gosnell et al., 2016), bays and lagoons (Horvat et al., 1999; Bloom et al., 2004; Stoichev et al., 2016) is focused mainly on contaminated zones worldwide.

The Adour Estuary (SW France) is medium size dynamic mesotidal estuary. Its urban/industrial downstream part is deteriorated due to numerous anthropogenic impacts (SDAGE-PDM, 2014; Cavalheiro et al., 2017). Both surface sediments (Stoichev et al., 2004) and water (Stoichev et al., 2006) from the Adour estuary were found to be moderately contaminated with Hg species with numerous sources situated in the downstream urban area. The concentrations of Hg species in local wastewaters in Adour Estuary (Point, 2004) varied two to five orders of

* Corresponding authors.
E-mail addresses: tstoichevbg@yahoo.com (T. Stoichev), david.amouroux@univ-pau.fr (D. Amouroux).

https://doi.org/10.1016/j.marpolbul.2022.114400
Received 25 September 2022; Received in revised form 19 November 2022; Accepted 21 November 2022
Available online 30 November 2022

magnitude (dissolved and particulate, respectively), which should be investigated, especially in light of possible bioaccumulation. Higher anthropogenic impact on European eels in Adour estuary occurred downstream compared to upstream sites (Arleny et al., 2007). However, unlike other coastal systems (Aly et al., 2013; Stoichev et al., 2018), the Adour estuary hydrodynamics efficiently exports pollutants (Sharif et al., 2014; Stoichev et al., 2004; Azaroff et al., 2019) that would make it able to recover rapidly if pollution would stop. Largest water quality improvement occurs in regions, experiencing recent control on Hg emission (Driscoll et al., 2013) and, therefore, Adour Estuary (France) would be a possible example of coastal system in rapid recovery.

Multiple regression (MR) was used to separate biogeochemical processes of addition and removal of contaminants in water during estuarine mixing for case of single and strong upstream contamination source (Stoichev et al., 2016). However, in Adour Estuary, there are downstream contamination sources, complicating the separation of biogeochemical variables. As a strategy, categorical variables (factors) were included, taking into account sample type and sampling time. Water from different upstream and estuarine locations in Adour Estuary, as well as from urban tributaries, was collected during three sampling campaigns. The development of generalized additive models (GAM) allowed finding the combinations of factors and important continuous variables involved in IHg and MeHg variations. However, GAM consume degrees of freedom, lack simple analytical representation and were used here only as preliminary insight on the variables to be included in analysis of covariance (ANCOVA) models to study the variability of IHg and MeHg in different type of water samples and their eventual sources in the downstream part. The resulting simple spatial/temporal equations would depict the IHg and MeHg concentrations as additive functions of specific biogeochemical variables. Such approach, using both categorical and continuous variables, was already applied to model estuarine biogeochemistry of organic contaminants (Stoichev et al., 2021). Additionally, marked difference in land use between Adour and Nive (a downstream tributary) will allow some estimation on its possible effect on IHg and MeHg concentrations. The concentrations from this study and measured up to 20 years ago in estuarine (Stoichev et al., 2006; Sharif et al., 2014) and upstream water (Point, 2004) of Adour will be compared and discussed in light of decreased emissions.

2. Methods

2.1. Study area

The Adour River (South-West France, Gulf of Biscay) is 310 km long and has 6189 km^2 drainage area (Stoichev et al., 2006). Different soils have developed near Adour River: Luvisol, Cambisol, Podzol, Albeluvisol, but also calcaric soils (Calcisol, rendzic Leptosol and calcaric Fluvisol) (ESBN, 2005). Important tributary in the estuarine area of Adour is Nive with 850 km^2 drainage area (Fabre, 1998) and more homogeneous soil types – Cambisol and acid-organic Umbrisol (ESBN, 2005). The main difference between Adour and Nive is related to land use. The Nive usually drains forested areas, small size farming and small urban zones. Industry, intense agriculture and bigger urban centers (Pau, Tarbes, Mont-de-Marsan, Dax, Lourdes) are situated along the Adour River watershed, inducing more important contamination with nitrates, pesticides and organic compounds of Adour compared to Nive (SDAGE-PDM, 2014). The average river discharge of Adour is about 350 $m^3\ s^{-1}$ and it is the third largest freshwater inflow to Bay of Biscay (Borja et al., 2019) while for Nive it is 25 $m^3\ s^{-1}$ (Point et al., 2003).

The Adour Estuary has narrow estuarine channel (about 500 m width, down to 200 m at the mouth) with almost no intertidal area, resulting in a short residence time (hours to days) of water and particles (Point et al., 2007). Tidal amplitude is between 2 and 5 m with influence observed up to 70 km upstream. Significant urban and industrial activities are located on the estuarine shores including sewage treatment, wood industry, waste incineration, electronics, metallurgy, harbor and aquaculture. Despite the importance of the upstream sources, non-negligible downstream fluxes compared to upstream (IHg: 4 %, MeHg: 9 %) are transported at low river discharge from wastewaters (Point, 2004).

2.2. Sampling

Bulk water samples (up to 30 cm depth) were collected at decreasing tide within the tidal limit of the estuary on three occasions: May 2017 (representing flood period), September 2017 (dry conditions) and January 2018 (low temperatures) and kept in cool box until laboratory. The tide coefficients were between 78 (May) and 109 (Jan). The upstream samples (1, 2, 3, 4, Fig. 1) are considered as upstream references, representative of the Hg species delivery from rivers. The downstream estuarine samples (A, B, C, D), collected with a ship from the middle of the main channel, are situated in the urban area. Samples with high anthropogenic impact are collected in the estuary near outlets of water treatment plants (WTPs) "St Frédéric" (6) and "Pont de l'Aveugle" (8). Samples from urban tributaries before entering the estuary were Aritxague (7) and "Moulin d'Esbouc" (9, influenced by WTP "St Bernard"). Some biogeochemical characteristics (pH, O_2, water temperature (T), conductivity) were measured on site with multiparametric probe HANNA Instrumentsc® HI-9829 or calculated afterward (salinity (Sal)).

2.3. Experimental

2.3.1. Cleaning procedures for Hg speciation

All materials were cleaned using ultra-trace protocol (Bravo et al., 2018). Water (1 L) was collected in polypropylene and stored in Teflon® bottles. All bottles and vials for sampling and analysis were first cleaned using detergents (RBS™) and rinsed thoroughly. It is then successively decontaminated in two baths of 10 % (v/v) nitric acid (HNO_3) and a bath of 10 % (v/v) hydrochloric acid (HCl) with rinsing steps (deionized water) between each bath. In each bath, the material undergoes a sonication step for a minimum of 2 h. Similar procedure was applied for decontamination of plastic caps but in 1 % acids for shorter time (15 min each bath). After rinsing with deionized water, all material was dried under a laminar flow hood and stored in plastic bags until use on site.

2.3.2. Sample pre-treatment for Hg speciation

One part of the sample was transferred into 250 mL Teflon® bottle then acidified with acetic acid (0.5–1 % depending on the particle load) for the analysis of Hg species. These samples correspond to the analysis of the total unfiltered fraction. The samples for determination of dissolved fraction (marked with subscript D) were filtered under vacuum (0.45 μm PVDF filters, Durapore). The filtrates were transferred and acidified similarly to total fraction with 0.5 % acetic acid. Samples are stored in the dark at 4 °C until extraction and analysis.

2.3.3. Chemical analysis

Mercury species concentrations were measured by capillary gas chromatography coupled to ICP-MS (GC Trace Ultra, XSerie II ICP-MS Thermo Scientific) after spiking with enriched 4stable isotopes of ^{199}IHg and ^{201}MeHg for species-specific isotope dilution analysis (Navarro et al., 2012; Bouchet et al., 2013; Sharif et al., 2014; Azad et al., 2019). Isotope tracer's solutions were prepared for each analytical session and their concentration was regularly determined by reverse isotope dilution. The Hg species were derivatized with sodium tetrapropylborate at pH 3.9 and extracted into 2,2,4-trimethylpentane. It should be noted that the filter-passing fraction contains both dissolved and most colloidal Hg species but will be referred to here as "dissolved" fraction for wording simplicity.

Quality assurance and quality control (QA/QC) was based on laboratory and field blanks, replicate analysis (Cavalheiro et al., 2016) and on repeated participations in international inter-laboratory comparisons (e.g. GEOTRACES inter-calibration cruises for Hg species in seawater).

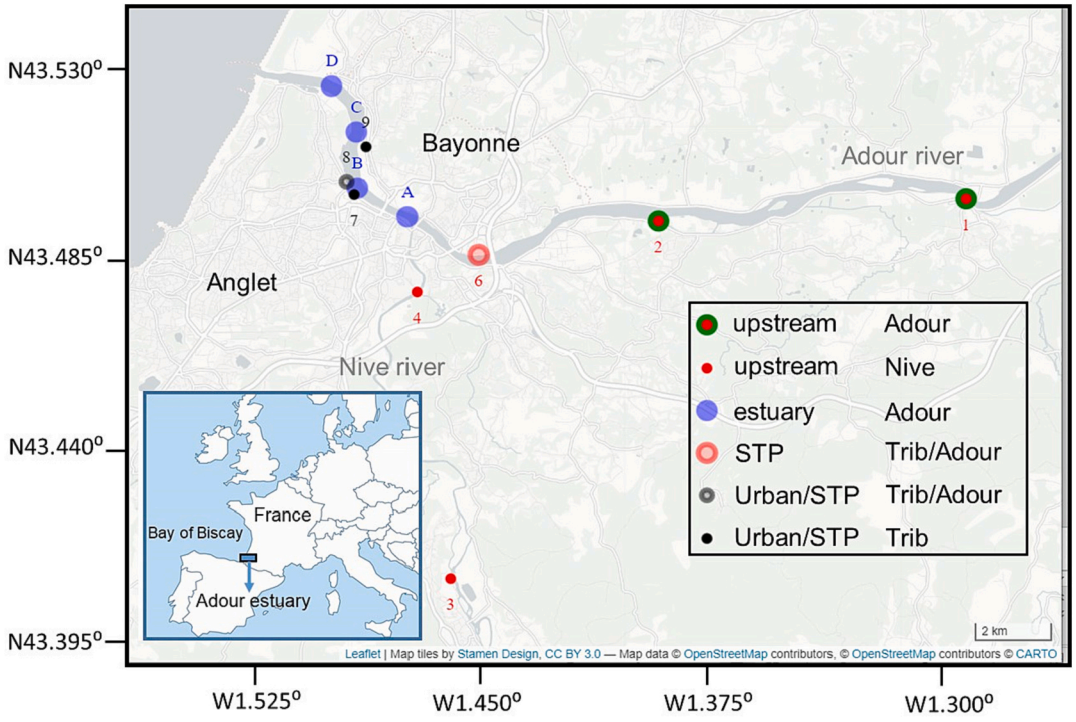

Fig. 1. Map of Adour estuary with sampling points. Sampling points separated according to type: upstream (1, 2, 3, 4), estuary (A, B, C, D), STP (6), Urban/STP (7, 8, 9), and place: Adour (1, 2, A, B, C, D), Trib/Adour (6, 8), Trib (7, 9), Nive (3, 4). The inset is map of France with Adour Estuary highlighted.

The repeatability was determined as average from all samples (unfiltered and filtered, n = 72) of the relative standard deviations (RSD) for the triplicate analysis and was 1.5 % for IHg and 3.4 % for MeHg. The limits of detection (LOD) were calculated using the results from the field blank samples and were similar for total and for dissolved Hg species. The limits of detection (LODs) for IHg_{DISS} and IHg were calculated as three times the standard deviation (SD) of the concentrations found in the blank samples. Since the $MeHg_{DISS}$ and MeHg were not detected in the blanks, the LODs in this case were estimated from 3 × SD of the background noise equivalent concentrations. For both total and dissolved species, the LODs were 0.03–0.07 ng L^{-1} and 3 pg L^{-1} for IHg and MeHg, respectively. The results for IHg_{DISS} and IHg were corrected with the average blank value.

The concentrations of total nitrogen (TN, mg L^{-1}) and dissolved organic carbon (DOC, mg L^{-1}) were determined in the filter-passing fraction (through 0.7 μm pre-combusted GF/F filters) by chemiluminescence and high temperature catalytic oxidation method, respectively, using a Shimadzu TOC-L CSH/CSN analyzer (Lee and Kim, 2018; García-Martín et al., 2021). Nutrient concentrations (μM) (phosphates (PO_4), nitrates (NO_3), nitrites (NO_2), ammonia (NH_4) and silicates (SiO_4)) were determined in the dissolved fraction (0.45 μm AC filters) by colorimetric procedures using a Shimadzu UV-1800 spectrophotometer (Koroleff, 1969; Mullin and Riley, 1955; Murphy and Riley, 1962; Strickland and Parsons, 1972). The concentrations of suspended particulate matter (SPM, mg L^{-1}), chlorophyll *a* (Chl, μg L^{-1}), and phaeopigments (Pha, μg L^{-1}) were determined in particulate fraction as previously described (Abril et al., 2002; Aminot and Kérouel, 2004; Lorenzen, 1967; Savoye et al., 2012). Particulate organic carbon (POC, % on particle weight basis or POC_V, mg L^{-1}, on sample volume basis) was measured after removal of carbonates by infrared spectroscopy via high temperature combustion on a Shimadzu TOC-L/SSM-5000A analyzer (Azaroff et al., 2019). δ13C and δ15N of particulate organic forms were measured using an elemental analyzer (Flash 2000, ThermoFisher Scientific) coupled with an isotope ratio mass spectrometer (IRMS, Isoprime, GV Instruments) (Savoye et al., 2003, 2012).

2.4. Statistical analysis

2.4.1. Preprocessing

The database is included in Supplementary materials (xlsx file). Dissolved and total concentrations of IHg, MeHg as well as the percentage of MeHg relative to total Hg (%MeHg) were dependent variables (Y_i). Biogeochemical characteristics were used as continuous explanatory variables (X_i). Active chlorophyll (actChl), ratio between Chl and POC ($R_{Chl/POC}$) and partition coefficient of organic carbon (K_{OC}) were also used as X_i:

$$ActChl = [Chl]/([Chl] + [Pha]) \quad (1)$$

$$R_{Chl/POC} = [Chl]/(10[SPM][POC]) \quad (2)$$

$$K_{OC} = 10^4[POC]/[DOC] \quad (3)$$

Other explanatory variables were categorical (factors). Factor "type" has four levels: effluents from Sewage Treatment Plant (STP), urban tributaries (Urban/STP), upstream and estuarine waters. In order to study the effect of Nive on the dependent variables, factor "place" was also included in the models. It has also four levels: "Adour", "Nive", "Trib" (samples from urban tributaries before entering the estuary) and "Trib/Adour" (samples near the outlet of urban tributaries with possible effect of the Adour estuarine water). Third factor in the models was "time" with levels May, September and January.

Continuous explanatory variables (average, geometric mean, range) are shown in Tables SI-1, SI-2 and SI-3 from Supplementary materials for different levels of factors "time", "type" and "place", respectively. Levels for place "Trib" and "Trib/Adour" are combined into one level "Trib_Trib/Adour" (Table SI-3), representing all urban stream samples. There is additional column regarding Adour upstream samples in order to compare with Nive. Significant difference ($p < 0.10$) for variables at different factor levels is studied with Wilcoxon rank sum test.

Local background levels (LBLs, Table SI-1) were calculated using "estuary" and "upstream" data as 90th percentiles contained within average ± 3σ intervals (where σ is the standard deviation), or as

averages from data contained within average ± 4σ intervals, for 3σ and 4σ methods, respectively (Gredilla et al., 2015). Ranges between 4σ and 3σ values are considered as LBL. The proportions (P) of samples with X_i equal to LBL, higher than LBL and lower than LBL are also presented (Tables SI-2, SI-3) with the respective binomial errors.

Statistical data treatment was carried out using R software (R Core Team, 2017). The dependent variables (Y_i) were represented as functions of q explanatory variables X_i. As required for linear models, both Y_i and X_i were normalized using graphical visualization of density function and Box-Cox transformations to give transformed variables Y_T and $X_{T,i}$:

$$Y_T = lnY \quad Y : \mathrm{IHg, MeHg, IHg_D, MeHg_D, \%MeHg} \tag{4a}$$

$$Y_T = \sqrt{Y} \quad Y : \mathrm{\%MeHg_D} \tag{4b}$$

$$X_T = lnX \quad X : \mathrm{NO_2, SiO_4, DOC, Chl, Pha, K_{OC}} \tag{5a}$$

$$X_T = \sqrt{X} \quad X : \mathrm{R_{Chl/POC}} \tag{5b}$$

$$X_T = 1/\sqrt{X} \quad X : \mathrm{Sal, O_2, PO_4, NO_3, NH_4,} \tag{5c}$$

$$X_T = 1/X \quad X : \mathrm{TN, POC} \tag{5d}$$

$$X_T = X \quad X : \mathrm{pH, T, SPM, ActChl, \delta13C, \delta15N} \tag{5e}$$

High correlations for transformed explanatory variables $X_{i,T}$ ($p < 10^{-5}$) were observed between O_2 and T, TN and NO_3, NH_4 and NO_2. Therefore, to avoid collinearity, part of X_i (O_2, NH_4, TN) were not considered.

The dependent variables (average, geometric mean, range) and dissolved fractions (F_D, %) are shown in Tables SI-4, SI-5 and SI-6 for different levels of factors "time", "type" and "place", respectively. Significant difference ($p < 0.10$) between groups studied with *t*-test on transformed dependent variables (Eqs. (4a), (4b)) and with Wilcox test on F_D. Like with X_i, LBLs (Table SI-4) and the proportion of samples with Y_i equal, higher and lower than LBL (Tables SI-5, SI-6) were calculated.

2.4.2. Analysis of variance

The effect of factor levels was determined by ANOVA with time/type and time/place initially included. Models were simplified by leaving only significant factors ($p < 0.1$). Factor levels with similar effects on $Y_{i,T}$ were combined. Thus, for each Y_i, specific levels determined factors time1, type1, place1. The obtained dependences and adjusted R^2 ($adjR^2$) are shown in Table SI-7. The effect of different factors was often additive and, in case some interaction exists, its mean square is at least an order of magnitude smaller than the mean squares for additive effects of both factors (Table SI-7 footnote).

2.4.3. Generalized additive models

Generalized additive models (GAM) were developed as a function of $X_{i,T}$ and of parametric terms – factors: "time1", "type1" or "place1" (Section 2.4.1). The factors were included in the intercept $a_0(\ldots)$ in the forms: a_0(time1), a_0(type1), a_0(place1), a_0(time1, type1) and a_0(time1, place1).

$$Y_T = a_0(\ldots) + s(X_{T,i})$$
$$\mathrm{X_i : pH, Sal, T, PO_4, NO_3, NO_2, SiO_4, DOC, Chl, Pha, SPM, POC, \delta13C, \delta15N, R_{Chl/POC}, ActChl, K_{OC}} \tag{6}$$

$$Y_T = a_0(\ldots) + s(Sal_T) + s(X_{T,i})$$
$$\mathrm{X_i : pH, PO_4, NO_3, NO_2, SiO_4, DOC, Chl, Pha, SPM, POC, \delta13C, \delta15N, R_{Chl/POC}, ActChl, K_{OC}} \tag{7}$$

$$Y_T = a_0(\ldots) + s(SPM_T) + s(X_{T,i})$$
$$\mathrm{X_i : PO_4, NO_3, NO_2, SiO_4, DOC, Chl, Pha, SPM, POC, \delta13C, \delta15N, R_{Chl/POC}, ActChl, K_{OC}} \tag{8}$$

Initially, all $X_{i,T}$ enter in GAM as smoothed functions (s). However, if their estimated degrees of freedom (edf) equal 1, they become parametric linear terms. If necessary, the number of factor levels in "time1", "type1" and "place1" is additionally decreased (Table SI-8, 117 models). The slope c_1 (should be near 1) and intercept c_0 (should be near 0) of the linear dependence between model (Y_{MOD}) and experimental (Y_{EXP}) values and the root mean square deviation of transformed variable ($RMSD_T$) for sample size n were calculated:

$$RMSD_T = \sqrt{\frac{\sum \left(Y_{EXP,T,i} - Y_{MOD,T,i}\right)^2}{n}} \tag{9}$$

Only models that showed significant effects ($p < 0.1$) and with $c_1 > 0.25$ were considered further and compared using analysis of deviance.

2.4.4. Linear models with continuous explanatory variables

In the linear models (LM), the relationship is expressed by L_1 or L_2, the index representing the highest interaction order, described in the starting model:

$$L_2\left(X_{T,1}, X_{T,2}, \ldots, X_{T,i}, \ldots, X_{T,q}\right) = \sum_{i=1}^{q} a_i X_{T,i} + \sum_{i \neq j} a_{i,j} X_{T,i} X_{T,j} \tag{10}$$

$$L_1\left(X_{T,1}, X_{T,2}, \ldots, X_{T,i}, \ldots, X_{T,q}\right) = \sum_{i=1}^{q} a_i X_{T,i} \tag{11}$$

The coefficients a_i and a_{ij} represent the simple terms for variable X_i and the double interactions, respectively. The specific indexing of the explanatory variables X_i is explained in Tables SI-8, SI-9 and SI-10. Higher order effects (quadratic and cubic for Sal and SPM; only quadratic for the rest of the variables) were checked for variables having significant simple effect. The number of coefficients in the starting models never exceeds 13 in order to avoid overparametrization (Crawley, 2007). Minimal adequate models were obtained by gradual deletion of non-significant terms (Stoichev et al., 2019). The stability of coefficients is studied by bootstrap with row resampling (online resources, Minimal Adequate ANCOVA) and equations with unstable coefficients are eliminated. Only equations with $c_1 > 0.5$ are included for further consideration.

One starting approach could be multiple regression (MR) with simple effects without interactions:

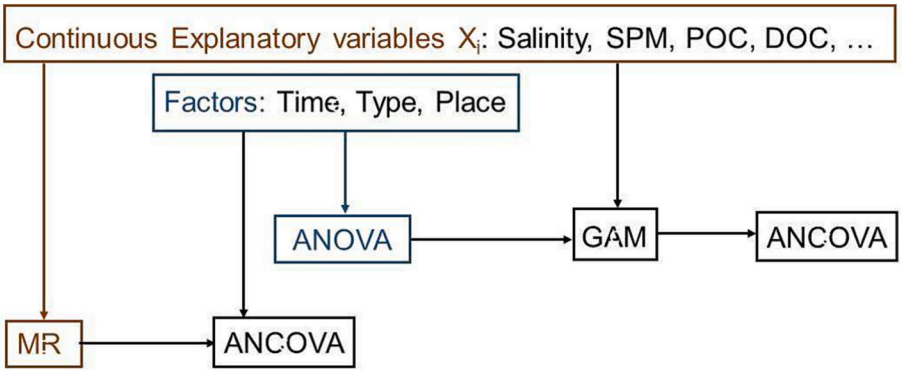

Fig. 2. Schema of used statistical models concerning factors (Analysis of Variance, ANOVA), continuous explanatory variables (Multiple Regression, MR) or both (Generalized Additive Models, GAM and Analysis of Covariance, ANCOVA).

$$Y_T = L_1\left(pH_T, Sal_T, T_T, PO_{4,T}, NO_{3,T}, NO_{2,T}, SiO_{4,T}, DOC_T, SPM_T, POC_T, \delta 13C_T, \delta 15N_T\right) \quad (12)$$

All equations with $RMSD_T$, c_1 and c_0 are presented in Table SI-9 (six models). Significant variables $X_{i,T}$ from MR equations were used for analysis of covariance (ANCOVA) by including factor-dependent intercepts: a_0(time), a_0(type), a_0(place), a_0(time, type), a_0(time, place). For each one of the five combinations of factors only simple effects or higher order effects of significant X_i were included but without interactions. Minimal adequate ANCOVA having more than two X_i were deleted.

Another starting approach is based on the same X_i as in the generalized additive model (GAM) equations (Table SI-8) to develop ANCOVA. The factors were also the same but with the original levels of "time", "type" and "place" (Fig. 1). All starting equations with two X_i have higher order effects of significant X_i and interaction terms. After stepwise simplification, only models with additive effects of X_i were included (Table SI-10, 60 models). Equations with factor "place" were not considered if separated levels "Trib" or "Trib/Adour" appeared because they were not important for the dependent variables Y_i. Schematic representation of the used models is shown in Fig. 2.

After preliminary evaluation of the dependences of Hg species concentrations from factors and biogeochemical variables, additional models for the MeHg, $MeHg_D$ and IHg_D were also developed from starting expressions:

$$ln[MeHg] = a_0(type) + L_2(IHg_T, POC_T) + (IHg_T)^2 + (POC_T)^2 \quad (13a)$$

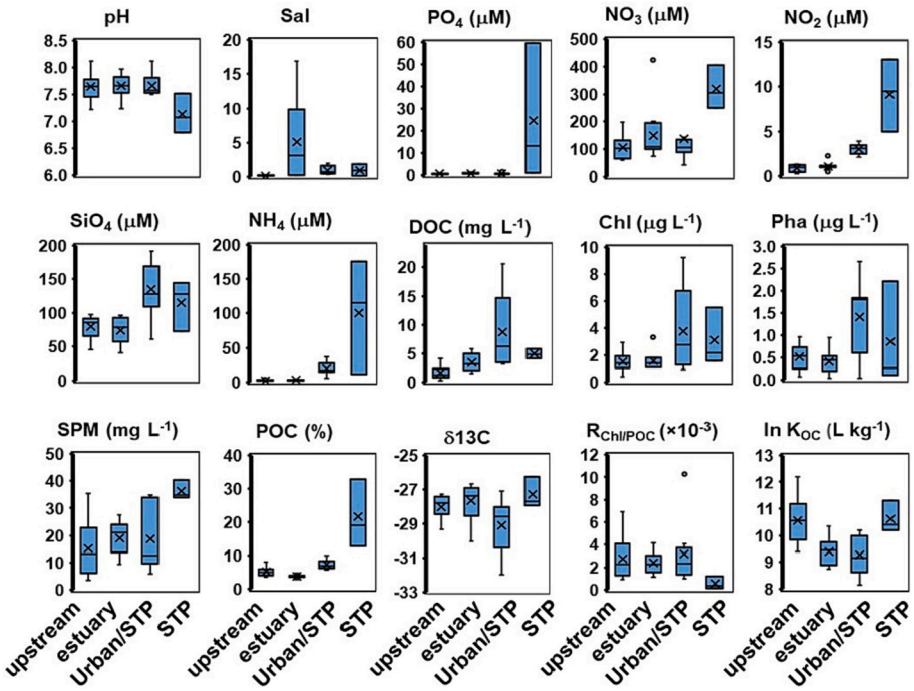

Fig. 3. Box-Whisker plot of biogeochemical variables in surface water from Adour Estuary separated according to sample type levels (Fig. 1, upstream (1, 2, 3, 4), estuary (A, B, C, D), STP (6), Urban/STP (7, 8, 9)). The box encompasses values between first (Q_1) and third (Q_3) quartiles. The median is marked with a line and × represents the average value. The error bar shows the range without outliers (for levels upstream, estuary and Urban/STP). A data is considered outlier if exceeds the distance of 1.5 times (Q_3–Q_1) bellow Q_1 or above Q_2. Only variables showing significant between type difference ($p < 0.1$) are selected.

$$ln[MeHg_D] = a_0(type) + L_2\left(IHg_{D,T}, X_{T,i}\right) + \left(IHg_{D,T}\right)^2 + \left(X_{T,i}\right)^2 + \left(X_{T,i}\right)^3 \quad (13b)$$

$$ln[IHg_D] = a_0(type) + L_2(IHg_T, POC_T) + (IHg_T)^2 + (POC_T)^2 \quad (13c)$$

The variables X_i are Sal or SPM for Eq. (13b). The same criteria for model simplification and selection as previously described were used (Supplementary materials, minimal adequate ANCOVA). The values of $RMSD_T$ for ANCOVA models (Table SI-10), selected for further consideration, are marked in bold.

3. Results

3.1. Factor-separated biogeochemical variables and concentrations of Hg species

Between-time differences of biogeochemical variables (Table SI-1) show that samples in May are characterized with higher DOC, low SPM, lower nutrient content and δ13C, having particulate organic matter rich in Chl due to phytoplankton development compared to Sept and Jan. Samples in Jan have more NO_3 and less Chl, δ15N and ActChl. Selected biogeochemical variables, grouped according to factor "type" (Table SI-2), demonstrating significant between-type differences, are shown in Fig. 3. The Adour Estuary is loading a low content of organic-rich suspended particles. Compared to upstream samples, estuarine ones have higher DOC and lower POC concentrations. Both Urban/STP and STP samples have more nutrients (NO_2, NH_4) and organic matter (DOC, POC) compared to upstream and estuarine samples. Therefore, important local downstream sources were observed, but they are rapidly diluted in the estuarine water. Samples from type "STP" (compared to Urban/STP) are particularly rich in all nutrients (except SiO_4), SPM and POC. Additionally, the organic matter in STP is more particle-associated and with low $R_{Chl/POC}$. Water from STP may have suffered slight oxygen depletion and is rich in CO_2 (lower pH) from partly oxidized organic matter. For most of the variables within Urban/STP (7, 8, 9, Fig. 1) between-site differences were not observed. However, POC was higher in site 7 (8.88 ± 1.08 %) compared to sites 8 and 9 combined (6.45 ± 0.56 %). Concentrations (μM) of NO_3 and NO_2 were higher in site 8 (NO_3: 228.5 ± 161.3; NO_2: 3.58 ± 0.36) compared to sites 7 and 9 combined (NO_3: 92.1 ± 27.8; NO_2: 2.72 ± 0.45). The effect of land use was studied by comparison between upstream water from Adour (agriculture area) and Nive (pristine area) Rivers, showing that Nive has less nutrients (NO_3, NO_2, PO_4) and its organic matter is more particle-associated (Table SI-3).

Between-time differences for Hg species concentrations (Table SI-4, Fig. 4) showed the lowest concentrations of IHg and IHg_D in May, probably due to lower SPM concentrations and higher in Sept, especially for Urban/STP stations. Although not significant, the highest concentrations of MeHg and $MeHg_D$ were observed in Sept. Significant variations of %MeHg and $\%MeHg_D$ (particularly high in May) were noticed. Higher average dissolved fraction F_D for IHg was observed in Jan (43 %) compared to May (30 %) and Sept (23 %), while, for MeHg, F_D was very stable over time (between 66 and 73 %).

Between-type differences (Fig. 4, Table SI-5) showed that "STP" have higher total IHg concentrations, all above the background levels, compared to the rest of the samples, while IHg_D concentrations do not fluctuate as much across type levels. Both MeHg and $MeHg_D$ showed significantly higher concentrations, all above the background levels, in STP compared to the rest of the sample type. Samples from STP have smaller average F_D of MeHg (46 %) compared to the rest of sample types (68–73 %). Within Urban/STP no significant differences between samples were observed except for $MeHg_D$, with lower concentration in site 8

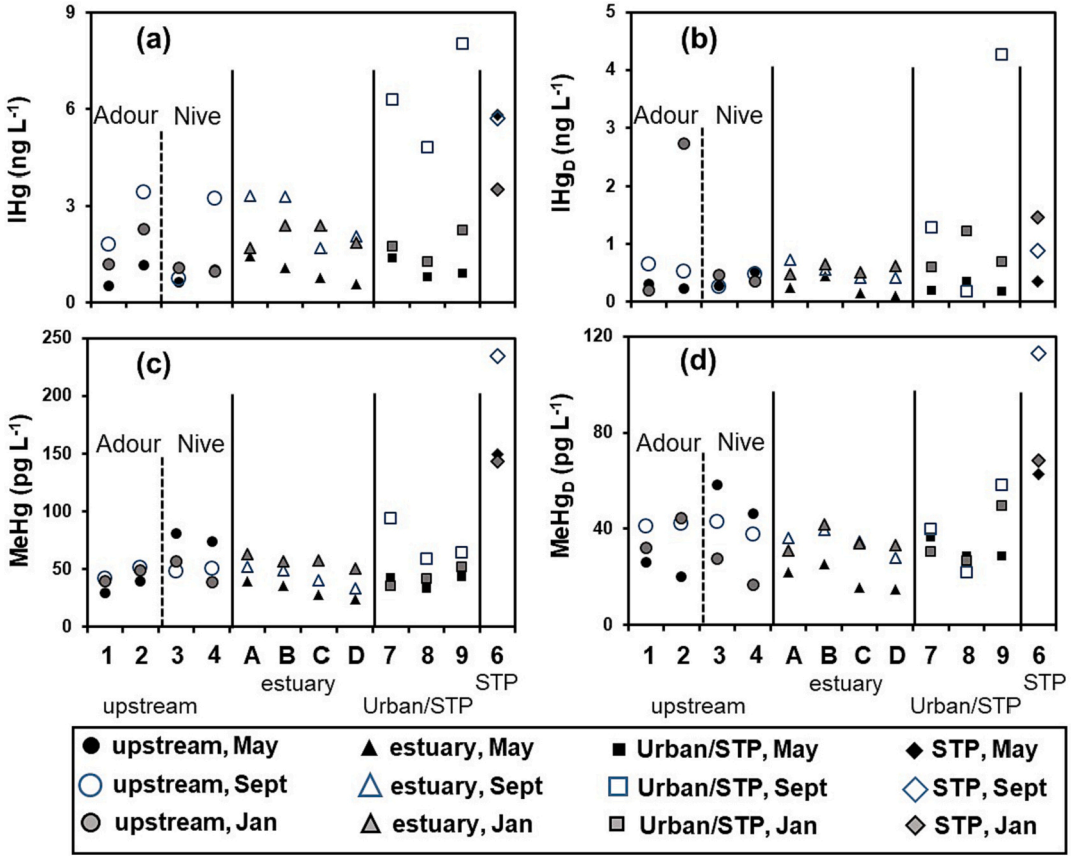

Fig. 4. Concentrations of IHg (a) total; (b) dissolved and of MeHg (c) total; (d) dissolved in surface water from Adour estuary. Samples (Fig. 1) grouped into upstream (Adour: 1, 2; Nive: 3, 4), estuary (A, B, C, D), Urban/STP (7, 8, 9) and STP (6) categories.

(26 ± 4 pg L^{-1}) compared to sites 7 and 9 combined (41 ± 11 pg L^{-1}). No significant difference was observed for total and dissolved IHg between upstream samples from Adour and Nive Rivers (Fig. 4). On the contrary, lower total MeHg and similar $MeHg_D$ concentrations were observed in Adour compared to Nive (Fig. 4, Table SI-6), which led to significant difference in average F_D for MeHg (81 % and 65 % in Adour and Nive Rivers, respectively).

The dependence between concentrations of Hg species and some biogeochemical variables for each sampling campaign (Fig. SI-1) shows that IHg is mainly carried by SPM while particulate organic matter and IHg determines the concentrations of MeHg. Salinity has no clear effect on Hg species concentrations in water from Adour Estuary.

3.2. Minimal adequate models to depict Hg species concentrations

The development of generalized additive models (GAM) allowed finding the combinations of factors and important transformed explanatory variables ($X_{i,T}$) to explain dependent variables (Y_i). However, GAM consume more degrees of freedom, lack simple analytical representation and here were used only as preliminary insight on the variables to be included in some starting ANCOVA models. Simple analytical expressions for Y_i were selected from Supplementary materials (minimal adequate ANCOVA). Eqs. (14)–(16) concern IHg and MeHg total concentrations:

$$ln[IHg] = a_0\left(time_{Sept(+)}; type_{Upstream(-)}\right) + |a_{11}|[SPM] - |a_{12}|\Big/[POC] \quad (14)$$

$$ln[MeHg] = a_0\left(type_{Urban/STP(-)}\right) + |a_{11}|[SPM] - |a_{12}|\Big/[POC] \quad (15)$$

$$ln[MeHg] = a_0\left(type_{Urban/STP(-)}\right) - |a_{12}|\Big/[POC] + |a_{18}|ln[IHg] \quad (16)$$

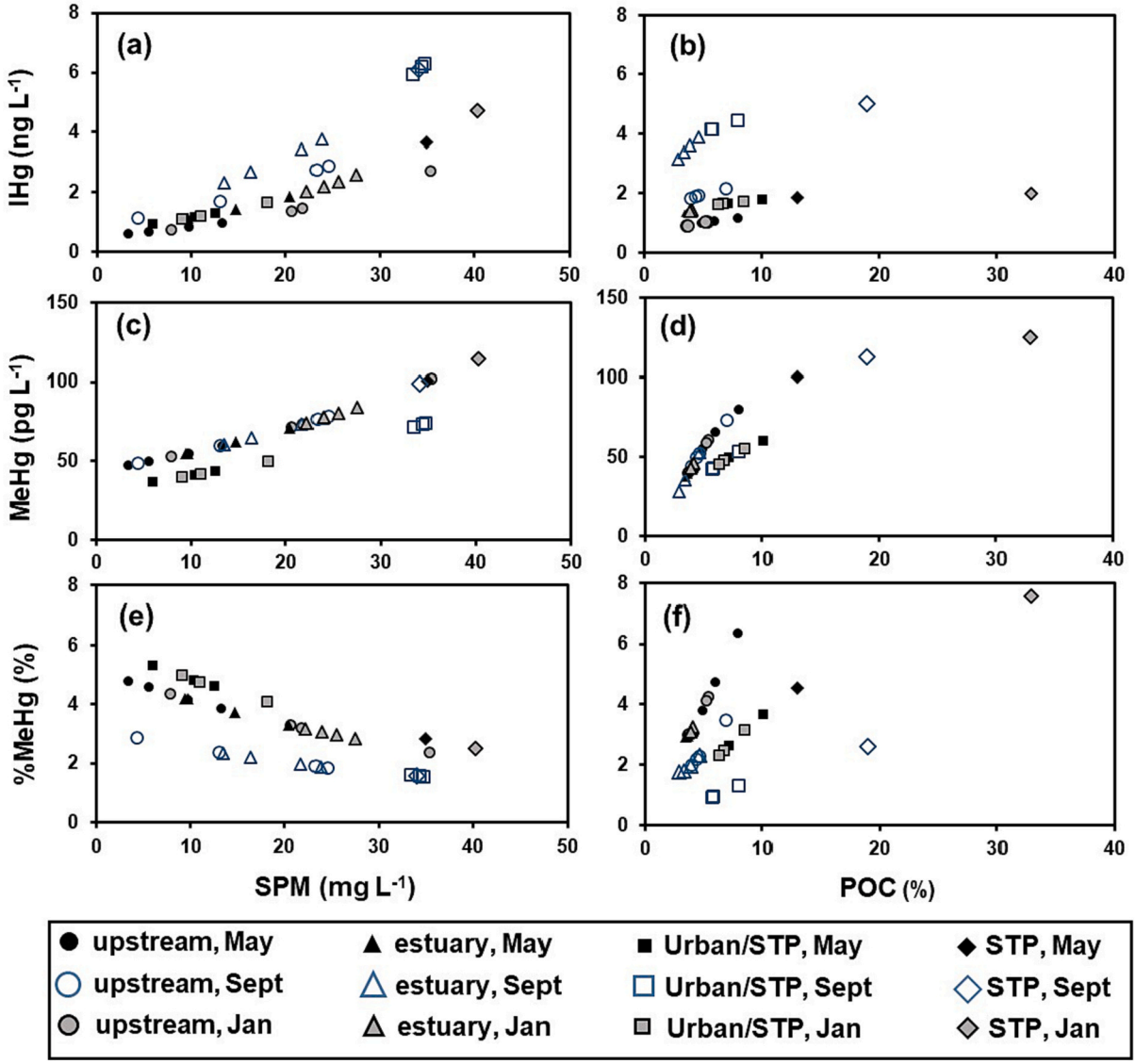

Fig. 5. Model values for total concentrations of (a, b) IHg (Eq. (14), adjR^2 = 0.836), (c, d) MeHg (Eq. (15), adjR^2 = 0.798), (e, f) percentage of MeHg relative to total Hg (%MeHg) (Eq. (17), adjR^2 = 0.756) in water (Adour Estuary) as a function of (a, c, e) changing SPM concentration at fixed POC and (b, d, f) changing POC concentration at fixed SPM. Fixed values for POC and SPM determined as group-based averages according to factor levels in the minimal adequate models. The slope c_1 for the dependence between model values and experimental values (a, b) 0.894 ± 0.067, (c, d) 0.809 ± 0.073 and (e, f) 0.694 ± 0.060.
$\ln[IHg] = a_0(time_{Sept(+)}; type_{Upstream(-)}) + |a_{11}|[SPM] - |a_{12}|/[POC]$.
$\ln[MeHg] = a_0(type_{Urban/STP(-)}) + |a_{11}|[SPM] - |a_{12}|/[POC]$.
$\ln[\%MeHg] = a_0(time_{Sept(-)}; type_{STPUrban/STP\ (-)}) - |a_{11}|[SPM] - |a_{12}|/[POC] + |a_{12,\ 12}|/[POC]^2$.

$$ln[\%MeHg] = a_0\left(time_{Sept(-)}; type_{STPUrban/STP\ (-)}\right) - |a_{11}|[SPM] - |a_{12}|\Big/[POC] + |a_{12,12}|\Big/[POC]^2 \quad (17)$$

The slope c_1 of the dependence between model and experimental values (Eqs. (14)–(16)) is between 0.81 and 0.89, except for %MeHg (Eq. (17), 0.69). The standard error of c_1 is in the range 6.2–9.0 % and adjR^2 is between 0.756 and 0.836. These models describe behavior of Y_i with range ratio of at least an order of magnitude.

For dissolved species, only models for $MeHg_D$ (Eqs. (18), (19)) match the selection criteria:

$$ln[MeHg_D] = a_0\left(type_{STP\ (+)}\right) + |a_2|\Big/\sqrt{Sal} - |a_{2,2}|\Big/Sal + |a_3|\ T \quad (18)$$

$$ln[MeHg_D] = a_0\left(type_{STP\ (+)}\right) - |a_{11}|[SPM] + |a_{11,11}|[SPM]^2 - |a_{11,11,11}|[SPM]^3 + |a_{19}|ln[IHg_D] \quad (19)$$

The slope c_1 is 0.67 with standard error 11.3 % (Eq. (18)) and 0.87 with standard error 7.1 % (Eq. (19)). As with the bulk samples, the models for Y_i in dissolved phase describe range ratios of an order of magnitude. However, the quality characteristics of models for dissolved concentrations are worse than those for total concentrations when only biogeochemical variables are used (Eq. (18)). For the same reason, no equations were selected for IHg_D.

In all equations, Y_i are functions of at least one factor. The total and dissolved concentrations of MeHg depend only on type and the concentrations of IHg – both on type and time. In all minimal adequate models, the interactions between continuous explanatory variables were checked, but the effects were always additive. The most important biogeochemical variables, affecting total concentrations of IHg, MeHg and %MeHg were SPM and POC (Eqs. (14), (15), (17)) which are statistically separated in Fig. 5. Such additive effects are separated by leaving one of the variables to vary while the others are fixed. Fixed

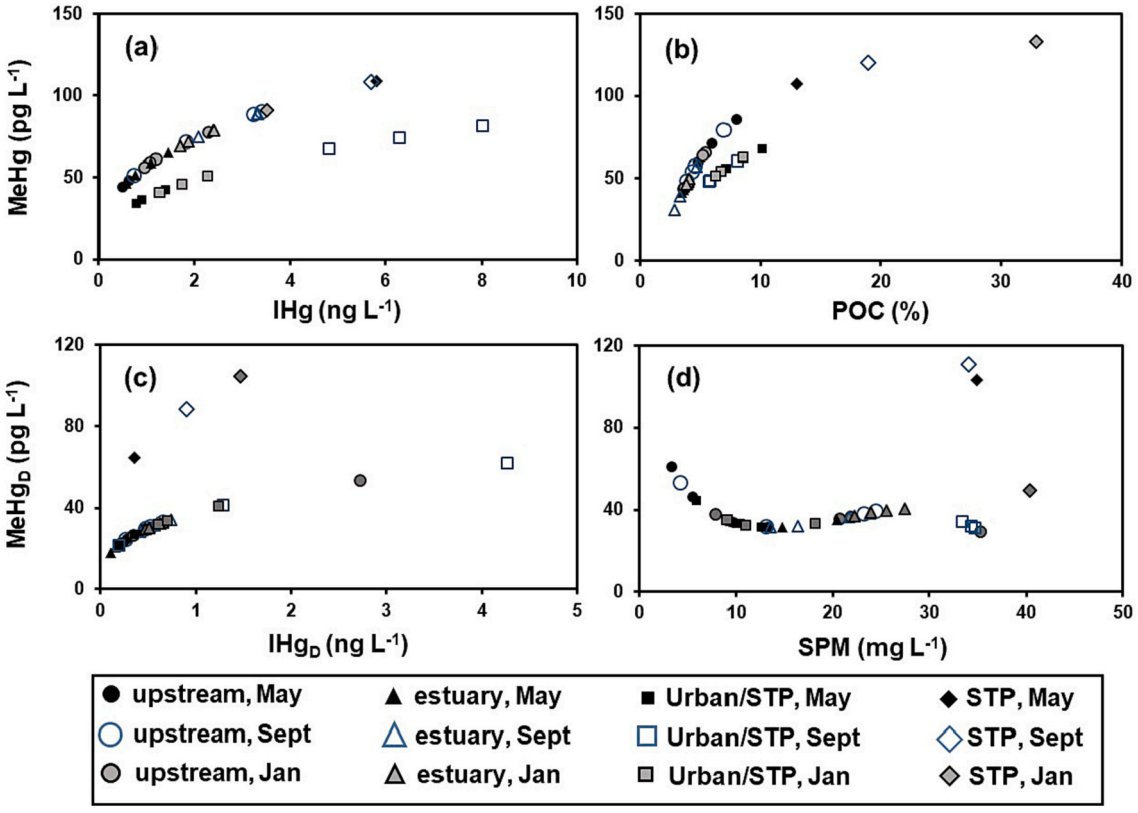

Fig. 6. Model values for concentrations of MeHg (a, b) total (Eq. (16), adjR^2 = 0.831) and (c, d) dissolved (Eq. (19), adjR^2 = 0.709) in water (Adour estuary) as a function of (a) changing IHg total concentration at fixed POC; (b) changing POC at fixed IHg total concentration; (c) changing IHg dissolved concentration at fixed SPM; (d) changing SPM at fixed IHg dissolved concentration Fixed values of dependent variables determined as group-based averages according to factor levels in the minimal adequate models. The slopes c_1 for the dependence between model values and experimental values are (a, b) 0.806 ± 0.050, (c, d) 0.872 ± 0.062.
$\ln[MeHg] = a_0(type_{Urban/STP(-)}) - |a_{12}|/[POC] + |a_{18}|\ \ln\ [IHg]$.
$\ln[MeHg_D] = a_0(type_{STP\ (+)}) - |a_{11}|[SPM] + |a_{11,\ 11}|[SPM]^2 - |a_{11,11,11}|[SPM]^3 + |a_{19}|\ \ln\ [IHg_D]$.

Table 1
Historical comparison of total mercury and methylmercury concentrations (geometric mean and *range*) in water from Adour Estuary. Data for previous studies filtered to salinity found here (0.1–16.9). Estimates of anthropogenic mercury emissions to the air (E) in France during the sampling years also presented.

Campaign	Salinity	Hg_{TOT} (ng L^{-1})[a]	MeHg (pg L^{-1})[a]	Emissions (E) (tons Hg $year^{-1}$)[b]	References
Febr 1998 (n = 5)	3.7 *(0.3–11.6)*	28.1 *(9.64–211.6)*	536 *(<762–2086)*	14.12	Stoichev et al., 2006
July 1998 (n = 6)	3.4 *(0.2–15.9)*	21.7 *(10.25–72.89)*	381 *(<762)*	14.12	
Sept 1999 (n = 18)	4.3 *(0.2–17)*	24.1 *(11.0–111.1)*	690 *(228–1285)*	12.83	
Febr 2001 (n = 9)	0.23 *(0.1–4.9)*	6.1 *(<0.54–194.8)*	37 *(<20–1189)*	10.88	
April 2007 May 2010 (n = 2)	0.42 *(0.2–0.9)*	2.03 *(1.52–2.70)*	77 *(48–124)*	5.05 *(4.78–5.34)*	Sharif et al., 2014
May 2017 (n = 4)	1.1 *(0.1–16.9)*	0.95 *(0.60–1.49)*	32 *(25–40)*	3.26	This study
Sept 2017 (n = 4)	0.69 *(0.1–10.8)*	2.54 *(1.74–3.38)*	43 *(34–52)*	3.26	
Jan 2018 (n = 4)	0.27 *(0.1–0.9)*	2.12 *(1.75–2.46)*	57 *(51–63)*	3.09	

Deposited mercury in France (2019) is derived from emissions from France (43.9 %) and from neighboring countries with similar environmental policies (46.1 %), similar emission trends as in France (https://www.emep.int/) and should be proportional to E. There is no effect of salinity on Hg_{TOT} geometric mean concentrations.
$\ln[Hg_{TOT}] = (-0.342 \pm 0.302) + (0.247 \pm 0.031)E$.
$AdjR^2 = 0.897$, n = 8.
[a] Concentrations lower than limit of detection (LOD) replaced by 0.5 * LOD to calculate geometric mean.
[b] https://www.citepa.org/fr/2021-hg/.

values of dependent variables were determined as group-based averages according to factor levels in the minimal adequate models. Similarly, the effects of Sal and T (Eq. (18)) on $MeHg_D$ were separated in Fig. SI-2 (Supplementary materials). In Figs. 5 and SI-2, the concentrations of Hg species are represented as simple functions of frequently measured biogeochemical variables. Nonetheless, in order to evaluate the effect of IHg precursors in the net methylation processes, the effects of IHg (and IHg_D) on total and dissolved MeHg concentrations, respectively, were separated from the effects of other biogeochemical variables X_i in Fig. 6.

4. Discussion

4.1. Recovery and long-term changes of Adour Estuary contamination by Hg compounds

Advanced technologies in WTPs and discontinuing use of Hg-containing products are expected to improve environmental water quality in Adour concerning Hg. Previous data on dissolved and particulate IHg, MeHg concentrations in Adour upstream (SPM 8 mg L^{-1}) and Nive (SPM 2 mg L^{-1}) Rivers from 2001 to 2002 are available (Point, 2004) and compared with total concentrations in May 2017 (with similar SPM values, Table SI-6 footnote). Despite slightly higher SPM values, four to seven times lower concentrations were measured in these rivers in May 2017 (e.g., in Adour upstream, 0.837 ng L^{-1} and 35 pg L^{-1} for IHg and MeHg, respectively) compared to 2001–2002 (3.50 ng L^{-1} and 231 pg L^{-1} for IHg and MeHg, respectively). Likewise, concentrations of Hg_{TOT} (sum of total IHg and MeHg) and MeHg in sample type "estuary" from this study (Table 1) are compared with previous data from Adour estuarine surface water with similar salinity range (0.1–16.9) as presented here (Stoichev et al., 2006; Sharif et al., 2014), and exhibit an important recovery of the estuary regarding Hg contamination. Concentrations of Hg_{TOT} for the period 1998–2018 were not related to salinity but to anthropogenic Hg emissions (E) to the environment such as in the air for France (https://www.citepa.org/fr/2021-hg/) during respective sampling year (Table 1). The variables E and Hg_{TOT} co-vary with time ($\ln[Hg_{TOT}]$ and E are strongly correlated, $p < 0.0005$), both having the greatest reduction during the first decade of the studied 20-year period. Such high correlation between Hg_{TOT} and emissions to the air (E) requires further explanation. Decrease of anthropogenic Hg emission to the atmosphere has been observed not only in France but also in all Europe (Driscoll et al., 2013). Therefore, important trans-border contamination is not expected, meaning changes of deposited Hg in France should be dependent on changes of E (https://www.emep.int/). Additionally, the emissions of metals within industrial effluents in France decreased between 2004 and 2018 (SDES-OFB et al., 2020), similarly to the other emissions to the environment. According to European Environment Agency, industrial releases of metals (including Hg) to water for the 27 member states were reduced by about 50 % between 2010 and 2017 (https://www.eea.europa.eu/ims). Therefore, the variations of emitted Hg to the air could be an indirect measure of changes of Hg, affecting aquatic environment, either from deposited Hg on soil or via direct point sources. The extrapolation of Hg_{TOT} concentrations in Adour estuarine waters (Table 1) to "zero" anthropogenic Hg emissions lead to a natural background concentration of 0.71 ± 0.21 ng L^{-1}. This value is only two to three times lower than current local background concentration of IHg (Table SI-4) thus, the Hg contamination in the Adour Estuary is getting closer to the modelled level for "pristine" aquatic environment. It is an example of a coastal system in recovery that rapidly responds to changes of anthropogenic Hg emissions due to its specific hydrodynamics. In contrast, the Aveiro Lagoon, although also in recovery, would require >300 years to reduce by 50 % the historical Hg pollution, localized in upstream area of the lagoon with more limited exchange with the ocean and receiving small freshwater flow (Pato et al., 2008; Stoichev et al., 2018).

4.2. Depicting IHg and MeHg concentrations in urban estuary by biogeochemical variables

Such low IHg concentrations would change the behavior of MeHg in the last 20 years. Previously, MeHg concentrations in Adour Estuary depended on biogeochemical variables but not on IHg concentrations (Stoichev et al., 2006). However, the transformed concentrations of MeHg in the current study are highly correlated with those of IHg in both dissolved ($p < 0.001$) and bulk samples ($p < 0.0001$) indicating that, at ng L^{-1} levels of IHg, MeHg depends not only on biogeochemical variables, such as POC (Fig. SI-1, Table SI-11), but is probably limited by IHg availability.

Separation of effects of SPM and POC for the total concentrations showed the transport of IHg and MeHg are similarly governed by mixing particles with different Hg content (Fig. 5). As observed in Bach Dang tropical estuary (Navarro et al., 2012), IHg is carried by particulate matter in Adour Estuary. Subsequently, IHg is involved in the production of MeHg as described by Eq. (16), which is equivalent to Eq. (15) (Fig. 6). Fine organic-rich particles carry preferably MeHg (compared to IHg) irrespectively of the sampling campaign. Thus, the %MeHg decreases with SPM and increases with POC. Similarly, particulate MeHg in Nalon Estuary is correlated with POC (Pavoni et al., 2021).

In dissolved phase, separation of effect of Sal and T showed that $MeHg_D$ concentrations slightly depend on salinity, showing possible remobilization at intermediate salinity (Fig. SI-2). The concentrations of $MeHg_D$ increased with T, explaining clearly higher $\%MeHg_D$ in warm seasons while no such effect was observed for %MeHg in the bulk phase (Table SI-4). The effect of SPM on $MeHg_D$ is separated from the influence of IHg_D as precursor for $MeHg_D$ production (Fig. 6). It demonstrates that,

at high SPM, lower $MeHg_D$ concentrations are expected, probably as a result from $MeHg_D$ sorption on particulate matter.

It was not possible to develop equations explaining variations of IHg_D neither by biogeochemical variables nor by including IHg concentration as explanatory variable (Eq. (13c)). Models describing IHg_D as function of SPM and non-linear function of IHg were developed (Supplementary materials equations). The best results were in the form:

$$[IHg_D] = [IHg] - d_1[SPM](1 - exp(-d_2[IHg])) \quad (20)$$

The slope c_1 for the dependence between model and experimental values of IHg_D is 0.733 ± 0.114. Thus, Eq. (20) is the only simple model for IHg_D (model values between 0 and [IHg]) that produces relatively good results. The coefficient $d_1 = 0.131 \pm 0.018$ represents maximum particulate concentration (μg g^{-1}) of IHg while $d_2 = 0.631 \pm 0.197$ is related to how steeply particulate concentration is increasing with increasing IHg total concentration before reaching saturation plateau. The non-linear effects (Fig. SI-3a, b) show that high SPM concentrations strongly limit the release of IHg in the dissolved form. Thus, despite higher concentration of IHg in STP samples, there is depletion of IHg_D due to much higher SPM concentration. Similar procedure developed for $MeHg_D$ as function of SPM and total MeHg concentrations demonstrated linear effects (Fig. SI-3c, d). Although $MeHg_D$ also decreases with SPM, IHg_D is retained on particles in much higher extent. Similarly, sorption of IHg_D on high concentrations of SPM was observed in Aveiro Lagoon while no such effect was noticed for $MeHg_D$ (Stoichev et al., 2016, 2018). Possibly, as in the Seine Estuary, high SPM concentrations induced flocculation of colloidal and sorption of truly dissolved IHg (Laurier et al., 2003). Preliminary results have shown that this process occurs at low salinity and low river discharge in the Adour Estuary and influences trace metals partitioning (Point, 2004).

Higher total concentrations were found near specific discharge points (0.79–8.02 ng L^{-1} and 34–235 pg L^{-1}) compared to those in upstream and estuarine samples (0.51–3.42 ng L^{-1} and 25–81 pg L^{-1} for IHg and MeHg, respectively). However, clear Hg contamination (MeHg, $MeHg_D$, IHg) was found only at the STP station (concentration higher than LBL, $P_+ = 100$ %, Table SI-5, Fig. 4), where high concentrations of organic-rich particles and nutrients were observed. The distinction between STP and the other sample types is even more noticeable for MeHg than for IHg. High total concentrations of IHg and MeHg in STP could be explained by more organic matter and SPM (Fig. 5) but they are only two to three times higher than the background values (Table SI-4) and have no great impact on estuarine water. Similarly, local wastewaters can be sources of musks and alkylphenols to Adour Estuary but have limited effect due to contaminants reactivity and a large dilution of these anthropogenic tributaries (Cavalheiro et al., 2017). The effect separation of Sal/T and SPM/IHg_D also shows concentrations of $MeHg_D$ in STP that are higher than expected, despite higher concentrations of SPM (Figs. 6, SI-2). The removal of IHg in WTPs is higher than that of MeHg (Stoichev et al., 2009). Therefore, effluent from STP (6, Fig. 1) might be slight source of MeHg to the Adour Estuary, probably as a result of more labile organic matter in STP station.

Higher MeHg concentrations with lower F_D were found in Nive than in Adour upstream (Fig. 4, Table SI-6). Despite much lower flowrate, Nive River transports about 9 % of MeHg to the estuary during dry periods (Point, 2004). Sediments from Nive River have less IHg and more MeHg than from Adour (Stoichev et al., 2004) suggesting higher MeHg accumulation or net methylation potentials, and explained by specific organic matter and total sulfur content in sediments. Thus, well defined maximum of MeHg concentration in Adour/Nive sediments have been observed at 0.3 % total S and 2.5–3.0 % organic C irrespectively of the sampling campaigns (Stoichev et al., 2004), while the concentrations of iHg were maximal at higher concentrations of both total S (0.4–0.7 %) and organic C (3.5 %). Lower DOC concentrations and particles richer in POC in Nive may be involved in higher particulate MeHg concentrations compared to Adour. Favorable microenvironment for methylation might occur near organic-rich particles (Ortiz et al., 2015). Alternatively, complexation of IHg with higher concentration of dissolved organic matter in Adour River (Table SI-3) would produce less reactive complexes (Stoichev et al., 2002) and decrease the availability for methylation.

5. Conclusions

The statistical effect separation by analysis of covariance was found useful to study IHg and MeHg biogeochemistry in estuary with possible downstream contamination sources. Reduced emissions of Hg rapidly decreased the contamination of estuarine water with Hg. Low Hg concentrations nowadays are modifying the extent of MeHg, becoming limited by IHg. Thus, both IHg and MeHg total concentrations are determined by organic-rich particles in a similar way, but the effect of organic matter is stronger for MeHg. Dissolved/colloidal concentrations, especially of IHg, decreased at high levels of SPM, possibly by sorption/flocculation. Total IHg and MeHg, found near specific discharge points, are carried by organic-rich particles and have negligible effect on estuarine water quality due to significant dilution. However, concentrations of dissolved MeHg near specific points are higher than predicted values, obtained by the statistical models, accounting for biogeochemical variables. The method efficiency is dependent upon availability of enough biogeochemical explanatory variables, and it is usually better for total than for dissolved concentrations. It is probable that more than two continuous variables are simultaneously required to explain dissolved concentrations. The utility of relating simple biogeochemical variables with IHg and MeHg concentrations should be checked for other estuaries affected by downstream contamination with Hg or with other contaminants.

Supplementary data to this article can be found online at https://doi.org/10.1016/j.marpolbul.2022.114400.

CRediT authorship contribution statement

Teodor Stoichev: Conceptualization, Methodology, Formal analysis, Writing. **Aubin Thibault de Chanvalon:** Conceptualization, Formal analysis, Methodology. **Sandrine Veloso:** Formal analysis, Investigation. **Jonathan Deborde:** Investigation. **Emmanuel Tessier:** Investigation. **Laurent Lanceleur:** Investigation. **David Amouroux:** Conceptualization, Funding acquisition, Investigation.

Declaration of competing interest

The authors declare that they have no known competing financial interests or personal relationships that could have appeared to influence the work reported in this paper.

Data availability

Data will be made available on request.

Acknowledgements

This work has been performed in the framework of the MICROPOLIT project supported by UPPA/CNRS, the New Aquitaine Region and the Adour-Garonne Water Agency (AEAG). This work is a contribution to the MESMIC Hub (I-Sites, E2S/UPPA). The authors acknowledge Fundação para a Ciência e a Tecnologia (FCT) for the Strategic Funding

UIDB/04423/2020 and UIDP/04423/2020 through national funds provided by FCT and European Regional Development Fund (ERDF) as well as the research contract of T.S.

References

Abril, G., Nogueira, M., Etcheber, H., Cabeçadas, G., Lemaire, E., Brogueira, M.J., 2002. Behaviour of organic carbon in nine contrasting european estuaries. Est. Coast. Shelf Sci. 54, 241–262.

Aly, W., Williams, I.D., Hudson, M.D., 2013. Metal contamination in water, sediment and biota from a semi-enclosed coastal area. Environ. Monit. Assess. 185, 3879–3895.

Aminot, A., Kérouel, R., 2004. Dissolved organic carbon, nitrogen and phosphorus in the N-E Atlantic and the N-W Mediterranean with particular reference to non-refractory fractions and degradation. Deep-Sea resPart I Oceanogr. Res. Pap. 51, 1975–1999.

Arleny, I., Tabouret, H., Rodriguez-Gonzalez, P., Bareille, G., Donard, O.F.X., Amouroux, D., 2007. Methylmercury bioconcentration in muscle tissue of the European eel (Anguilla anguilla) from the Adour estuary (Bay of Biscay, France). Mar. Pollut. Bull. 54, 1031–1036.

Azad, A.M., Frantzen, S., Bankt, M.S., Johnsen, I.A., Tessier, E., Amouroux, D., Madsen, L., Maage, A., 2019. Spatial distribution of mercury in seawater, sediment, and seafood from the Hardangerfjord ecosystem. Norway. Sci. Total Environ. 667, 622–637.

Azaroff, A., Tessier, E., Deborde, J., Guyoneaud, R., Monperrus, M., 2019. Mercury and methylmercury concentrations, sources and distribution in submarine canyon sediments (Capbreton, SW France): implications for the net methylmercury production. Sci. Total Environ. 673, 511–521.

Balcom, P.H., Hammerschmidt, C.R., Fitzgerald, W.F., Lamborg, C.H., O'Connor, J.S., 2008. Seasonal distributions and cycling of mercury and methylmercury in the waters of New York/New Jersey Harbor estuary. Mar. Chem. 109, 1–17.

Bloom, N.S., Moretto, L.M., Ugo, P., 2004. A comparison of the speciation and fate of mercury in two contaminated coastal marine ecosystems: the Venice lagoon (Italy) and Lavaca Bay (Texas). Limnol. Oceanogr. 49, 367–375.

Borja, A., Amouroux, D., Anschutz, P., Gómez-Gesteira, M., Uyarra, M.C., Valdés, L., 2019. The Bay of Biscay. In: Sheppard, C. (Ed.), World Seas: An Environmental Evaluation, , Second editionVolume One. Elsevier, Europe, The Americas and West Africa, pp. 113–152.

Bouchet, S., Amouroux, D., Rodriguez-Gonzalez, P., Tessier, E., Monperrus, M., Thouzeau, G., Clavier, J., Amice, E., Deborde, J., Bujan, S., Grall, J., Anschutz, P., 2013. MMHg production and export from intertidal sediments to the water column of a tidal lagoon (Arcachon Bay, France). Biogeochemistry 114, 341–358.

Bratkič, A., Ogrinc, N., Kotnik, J., Faganeli, J., Žagar, D., Yano, S., Tada, A., Horvat, M., 2013. Mercury speciation driven by seasonal changes in a contaminated estuarine environment. Environ. Res. 125, 171–178.

Bravo, A.G., Kothawala, D.N., Attermeyer, K., Tessier, E., Bodmer, P., Amouroux, D., 2018. Cleaning and sampling protocol for analysis of mercury and dissolved organic matter in freshwater systems. MethodsX 5, 1017–1026.

Cavalheiro, J., Sola, C., Baldanza, J., Tessier, E., Lestremau, F., Botta, F., Preud'homme, H., Monperrus, M., Amouroux, D., 2016. Assessment of background concentrations of organometallic compounds (methylmercury, ethyllead and butyl- and phenyltin) in french aquatic environments. Water Res. 94, 32–41.

Cavalheiro, J., Zuloaga, O., Prieto, A., Preudhomme, H., Amouroux, D., Monperrus, M., 2017. Occurrence and fate of organic and organometallic pollutants in municipal wastewater treatment plants and their impact on receiving waters (Adour Estuary, France). Arch. Environ. Contam. Toxicol. 73, 619–630.

Crawley, M.J., 2007. The R Book. Wiley, Chichester.

Driscoll, C.T., Mason, R.P., Chan, H.M., Jacob, D.J., Pirrone, N., 2013. Mercury as a global pollutant: sources, pathways, and effects. Environ. Sci. Technol. 47, 4967–4983.

ESBN, 2005. In: European Soil Bureau Network, Soil Atlas of Europe. European Commission, Office for Official Publications of the European Communities, L-2995 Luxembourg, p. 128.

Fabre, E., 1998. Aquatic hyphomycetes in three rivers of southwestern France. I. Spatial and temporal changes in conidial concentration, species richness, and community diversity. Can. J. Bot. 76, 99–106.

García-Martín, E.E., Sanders, R., Evans, C.D., Kitidis, V., Lapworth, D.J., Rees, A.P., et al., 2021. Contrasting estuarine processing of dissolved organic matter derived from natural and human-impacted landscapes. Glob. Biogeochem. Cycles 35, e2021GB007023.

Gosnell, K., Balcom, P., Ortiz, V., DiMento, B., Schartup, A., Greene, R., Mason, R., 2016. Seasonal cycling and transport of mercury and methylmercury in the turbidity maximum of the Delaware estuary. Aquat. Geochem. 22, 313–336.

Gredilla, A., Fdez-Ortiz de Vallejuelo, S., de Diego, A., Arana, G., Stoichev, T., Amigo, J. M., Wasserman, J.C., Botello, A.V., Sarkar, S.K., Schäfer, J., Moreno, C., de la Guardia, M., Madariaga, J.M., 2015. A chemical status predictor. A methodology based on world-wide sediment samples. J. Environ. Manag. 161, 21–29.

Horvat, M., Covelli, S., Faganeli, J., Logar, M., Mandić, V., Rajar, R., Širca, A., Žagar, D., 1999. Mercury in contaminated coastal environments; a case study: the Gulf of Trieste. Sci. Total Environ. 237 (238), 43–56.

Koroleff, F., 1969. Determination of ammonia as indophenol blue. In: International Council for the Exploration of the sea (ICES), p. 8.

Laurier, F.J.G., Cossa, D., Gonzalez, J.L., Breviere, E., Sarazin, G., 2003. Mercury transformations and exchanges in a high turbidity estuary: the role of organic matter and amorphous oxyhydroxides. Geochim. Cosmochim. Acta 67, 3329–3345.

Lee, S.-A., Kim, G., 2018. Sources, fluxes, and behaviors of fluorescent dissolved organic matter (FDOM) in the Nakdong River estuary, Korea. Biogeosciences 15, 1115–1122.

Leermakers, M., Galletti, S., De Galan, S., Brion, N., Baeyens, W., 2001. Mercury in the southern North Sea and scheldt estuary. Mar. Chem. 75, 229–248.

Liu, M., Zhang, Q., Maavara, T., Liu, S., Wang, X., Raymond, P.A., 2021. Rivers as the largest source of mercury to coastal oceans worldwide. Nat. Geosci. 14, 672–677.

Lorenzen, C., 1967. Determination of chlorophyll and pheo-pigments: spectrophotometric equations. Limnol. Oceanogr. 12, 343–346.

Mullin, J.B., Riley, J.P., 1955. The colorimetric determination of silicate with special reference to sea and natural waters. Anal. Chim. Acta 12, 162–176.

Murphy, J., Riley, J.P., 1962. A modified single solution method for determination of phosphate in natural waters. Anal. Chim. Acta 27, 31–36.

Navarro, P., Amouroux, D., Thanh, N.D., Rochelle-Newall, E., Ouillon, S., Arfi, R., Van, T. C., Mari, X., Torréton, J.-P., 2012. Fate and tidal transport of butyltin and mercury compounds in the waters of the tropical Bach Dang Estuary (Haiphong, Vietnam). Mar. Pollut. Bull. 64, 1789–1798.

Ortiz, V.L., Mason, R.P., Ward, J.E., 2015. An examination of the factors influencing mercury and methylmercury particulate distributions, methylation and demethylation rates in laboratory-generated marine snow. Mar. Chem. 177, 753–762.

Pato, P., Lopes, C., Válega, M., Lillebø, A.I., Dias, J.M., Pereira, E., Duarte, A.C., 2008. Mercury fluxes between an impacted coastal lagoon and the Atlantic Ocean. Est. Coast. Shelf Sci. 76, 787–796.

Pavoni, E., García-Ordiales, E., Covelli, S., Cienfuegos, P., Roqueñí, N., 2021. Legacy of past mining activity affecting the present distribution of dissolved and particulate mercury and methylmercury in an estuarine environment (Nalón River, Northern Spain). Appl. Sci. 11, 4396.

Point, D., 2004. In: Spéciation et biogéochimie des éléments traces métalliques dans l'estuaire de l'Adour. Université de Pau et des Pays de l'Adour, p. 340. PhD thesis.

Point, D., Bareille, G., Amouroux, D., Etcheber, H., Donard, O.F.X., 2007. Reactivity, interactions and transport of trace elements, organic carbon and particulate material in a mountain range river system (Adour River, France). J. Environ. Monit. 9, 157–167.

Point, D., Bareille, G., Stoichev, T., Amouroux, D., Donard, O.F.X., 2003. Trace metals inputs in the Adour urban estuary: influence and impact of human pressure. J. Phys. 107, 1071–1074. IV, Volume II, Boutron, C., Ferrari, C. (Eds.).

R Core Team, 2017. R: A language and environment for statistical computing. Vienna, Austria: R Foundation for Statistical Computing. Retrieved from. http://www.R-project.org/.

Savoye, N., Aminot, A., Tréguer, P., Fontugne, M., Naulet, N., Kérouel, R., 2003. Dynamics of particulate organic matter δ15N and δ13C during spring phytoplankton blooms in a macrotidal ecosystem (Bay of Seine, France). Mar. Ecol. Prog. Ser. 255, 27–41.

Savoye, N., David, V., Morisseau, F., Etcheber, H., Abril, G., Billy, I., Charlier, K., Oggian, G., Derriennic, H., Sautour, B., 2012. Origin and composition of particulate organic matter in a macrotidal turbid estuary: the Gironde Estuary,France. Est. Coast. Shelf Sci. 108, 16–28.

SDAGE-PDM, 2014. In: Synthese de l'actualisation de l'état des lieux du SDAGE 2016–2021. Comité de bassin Adour-Garonne (validée le 02 décembre 2013), Commission territoriale Adour. Le Schema Directeur d'Amenagement et de Gestion des Eaux (SDAGE) et son Programme De Mesures (PDM), p. 31.

SDES-OFB, Joassard, I., Bréjoux, E., Larrieu, C., Dequesne, J., 2020. In: Eau et milieux aquatiques, les chiffres clés. Le Service des Données et Études Statistiques (SDES) en partenariat avec l'Office Français de la Biodiversité (OFB), Ministère de la Transition Écologique, p. 127.

Sharif, A., Monperrus, M., Tessier, E., Bouchet, S., Pinaly, H., Rodriguez-Gonzalez, P., Maron, P., Amouroux, D., 2014. Fate of mercury species in the coastal plume of the Adour River estuary (Bay of Biscay, SW France). Sci. Total Environ. 496, 701–713.

Stoichev, T., Amouroux, D., Monperrus, M., Point, D., Tessier, E., Bareille, G., Donard, O. F.X., 2006. Mercury in surface waters of a macrotidal urban estuary (River Adour, south-West France). Chem. Ecol. 22, 137–148.

Stoichev, T., Amouroux, D., Wasserman, J., Point, D., de Diego, A., Bareille, G., Donard, O.F.X., 2004. Dynamics of mercury species in surface sediments from a macrotidal estuarine-coastal system (Adour River, Bay of Biscay). Est. Coast. Shelf Sci. 59, 511–521.

Stoichev, T., Martin-Doimeadios, R.C.R., Amouroux, D., Molenat, N., Donard, O.F.X., 2002. Application of cryofocusing hydride generation and atomic fluorescence detection for dissolved mercury species determination in natural water samples. J. Environ. Monit. 4, 517–521.

Stoichev, T., Tessier, E., Almeida, C.M., Basto, M.C.P., Vasconcelos, V.M., Amouroux, D., 2018. Flux model to estimate the transport of mercury species in a contaminated lagoon (Ria de Aveiro, Portugal). Environ. Sci. Pollut. Res. 25, 17371–17382.

Stoichev, T., Tessier, E., Amouroux, D., Almeida, C.M., Basto, M.C.P., Vasconcelos, V.M., 2016. Multiple regression analysis to assess the role of plankton on the distribution and speciation of mercury in water of a contaminated lagoon. J. Haz. Mater. 318, 711–722.

Stoichev, T., Tessier, E., Coelho, J.P., Lobos Valenzuela, M.G., Pereira, M.E., Amouroux, D., 2019. Multiple regression analysis to assess the spatial distribution and speciation of mercury in surface sediments of a contaminated lagoon. J. Haz. Mater. 367, 715–724.

Stoichev, T., Marques, A., Almeida, C.M., 2021. Modeling the relationship between emerging and persistent organic contaminants in water, sediment and oysters from a temperate lagoon. Mar. Pollut. Bull. 164, 111994.

Stoichev, T., Tessier, E., Garraud, H., Amouroux, D., Donard, O.F.X., Tsalev, D.L., 2009. Mercury speciation and partitioning along a municipal sewage treatment plant. J. Balkan Ecol. 12, 135–145.

Strickland, J.D.H., Parsons, T.R., 1972. A practical handbook of seawater analysis. In: Fisheries Research Board of Canada Bulletin 167, Fisheries Research Board of Canada, Ottawa.

Wang, S., Jia, Y., Wang, S., Wang, X., Wang, H., Zhao, Z., Liu, B., 2009. Total mercury and monomethylmercury in water, sediments, and hydrophytes from the rivers, estuary, and bay along the Bohai Sea coast, northeastern China. Appl. Geochem. 24, 1702–1711.